

Fault-tolerant mixed boundary punctures on the toric code

Yao Shen(沈尧), Fu-Lin Zhang(张福林)

Citation: Chin. Phys. B. 35, 090211 (2026). DOI: 10.1088/1674-1056/ae5c78 | CSTR: 32038.14.CPB.ae5c78
http://cpb.iphy.ac.cn; http://iopscience.iop.org/cpb

What follows is a list of articles you may be interested in

Manipulation of the Majorana Ising spin via Rashba–Dresselhaus spin–orbit coupling

Lili Liu(刘利利), Qi-Sheng Xu(徐其胜), Cai Chen(陈才), Chui-Zhen Chen(陈垂针), Dong-Hui Xu(许东辉)
Chin. Phys. B. 35, 067404 (2026). DOI: 10.1088/1674-1056/ae43cd | CSTR: 32038.14.CPB.ae43cd

Quantum toric code decoding method based on syndrome-preliminary error fusion module and ResNet architecture

Nai-Hua Ji(纪乃华), Ping-Li Song(宋平俐), Wei Wang(王伟), Hui-Qian Sun(孙汇倩), Hong-Yang Ma(马鸿洋)
Chin. Phys. B. 35, 060303 (2026). DOI: 10.1088/1674-1056/ae1818 | CSTR: 32038.14.CPB.ae1818

Dicke–Ising quantum battery of an ion chain driven by a mechanical oscillator

Jun Wen(文军), Zheng Wen(文政), Ping Peng(彭娉), Guan-Qiang Li(李冠强)
Chin. Phys. B. 34, 100302 (2025). DOI: 10.1088/1674-1056/add50d | CSTR: 32038.14.CPB.add50d

---

Fault-tolerant mixed boundary punctures on the toric code

Yao Shen(沈尧)[1,†] and Fu-Lin Zhang(张福林)[2]

[1] *School of Criminal Investigation, People's Public Security University of China, Beijing* 100038, *China*
[2] *Department of Physics, School of Science, Tianjin University, Tianjin* 300072, *China*

(Received 11 February 2026; revised manuscript received 31 March 2026; accepted manuscript online 8 April 2026)

Defects on the toric code, a well-known exactly solvable Abelian anyon model, can exhibit non-Abelian statistical properties, which can be classified into punctures and twists. Benhemou *et al.* [*Phys. Rev. A* **105** 042417 (2022)] introduced a mixed boundary puncture model that integrates the advantages of both punctures and twists. They proposed that non-Abelian properties could be realized in the symmetric subspace $\{|{+}{+}\rangle, |{-}{-}\rangle\}$. This work demonstrates that the nontrivial antisymmetric subspace $\{|{+}{-}\rangle, |{-}{+}\rangle\}$ also supports non-Abelian statistics. The mixed boundary puncture model is shown to be fault-tolerant in both subspaces, offering resistance to collective dephasing noise and collective rotation noise. In addition, we propose and validate a quantum information masking scheme within the three-partite mixed boundary puncture model.

Keywords: toric code, Kitaev anyon, Ising anyon

PACS: 02.70.–c

DOI: 10.1088/1674-1056/ae5c78 **CSTR:** 32038.14.CPB.ae5c78

1. Introduction

In 1997, Kitaev[1] proposed a topological code, known as the toric code or surface code, depending on the boundary conditions. Typically defined on a boundaryless surface, the toric code's low-energy excitations are Abelian anyons.[2–5] The braiding group representation of Abelian anyons is a one-dimensional irreducible representation; however, topological quantum computation (TQC) generally requires two-dimensional or higher representations to implement quantum gate operations. This limitation makes the toric code, in its basic form, generally unsuitable for TQC.

Nevertheless, defects on the toric code can introduce non-Abelian statistics,[6,7] overcoming this limitation and making the toric code an important platform for TQC.[8–17] The toric code includes both local (point-like) defects[18–22] and nonlocal (line-like or twist) defects.[23–26] Punctures are local holes in the lattice, whereas twists correspond to the endpoints of nonlocal domain walls. Their behavior closely resembles that of Majorana zero modes.[23,24,27–29] Recently, Benhemou *et al.*[7] studied the hybridization of these two defects, effectively combining their advantages and demonstrating the presence of non-Abelian statistics in Ising anyons. In this framework, information is encoded in nonlocal degrees of freedom, and universal quantum gates can be realized through braiding and fusion operations.

The toric code utilizes its topological properties to protect qubits from certain types of errors, making it a promising platform for fault-tolerant quantum computation. First, toric code punctures exhibit a high fault-tolerance threshold of around 1%, meaning that increasing the code distance (i.e., enlarging the size of the surface code) can significantly reduce logical error rates.[30–32] Second, the toric code only requires parity checks between nearest neighbors, simplifying its implementation in physical systems.[8–10] As a result, topological quantum systems are highly competitive due to their combination of a high fault-tolerance threshold, accuracy, and minimal qubit overhead. The toric code plays a crucial role in TQC, offering unique encoding schemes and robust error correction. Therefore, it is not only a key component in TQC but also an important focus of research in quantum computing.

This work builds upon the research of Benhemou *et al.*[7] by demonstrating mixed boundary punctures and realizing non-Abelian statistics in the nontrivial antisymmetric subspace $\{|{+}{-}\rangle, |{-}{+}\rangle\}$, while Benhemou *et al.* proposed the realization in the symmetric subspace $\{|{+}{+}\rangle, |{-}{-}\rangle\}$. These two subspaces are independent of each other, distinguished by their respective realization methods within the lattice model. We show that both systems are immune to two typical types of noise — collective dephasing and collective rotation — within their respective subspaces. Consequently, these two subspaces of the mixed boundary punctures on the toric code are fault-tolerant. This conclusion highlights the significant potential of non-Abelian statistics in the context of the Abelian lattice model for TQC. Additionally, we propose and validate a quantum information masking scheme applicable to the three-partite mixed boundary puncture model.

In Section 2, we present the Abelian and non-Abelian anyon models, along with the mixed boundary punctures model. Section 3 discusses the robustness of the mixed bound-

†Corresponding author. E-mail: shenyaophysics@hotmail.com; shenyao@ppsuc.edu.cn

© 2026 Chinese Physical Society and IOP Publishing Ltd. All rights, including for text and data mining, AI training, and similar technologies, are reserved.

ary punctures model against two types of collective noise. In Section 4, we design the information masking scheme within the mixed boundary punctures model. Finally, we provide a summary in Section 5.

2. Mixed boundary punctures

2.1. Anyon models

The unitary modular tensor category is the algebraic structure describing the general anyon system. The total anyonic space consists of all Hilbert subsystem spaces and the fusion spaces of all charges[1–5]

$$H_{ab}^{c} = \underset{ab}{\oplus} H_a \otimes H_b \otimes V_{ab}^{c}, \tag{1}$$

where H_a represents the Hilbert subspace of charge a, and V_{ab}^{c} is the fusion space containing the fusion rules. In the fusion space V_{ab}^{c}, the fusion rule seems like a superposition.

$$a \otimes b = \underset{c\in L}{\oplus} N_{ab}^{c} c, \tag{2}$$

where $a, b \in L$ and N_{ab}^{c} are the possible ways of fusing a and b. The matrix relating two different bases of the splitting trees is the F-symbol. The braiding action is called the R-symbol (see Fig. 1). The algebraic model of anyons is composed of the fusion rules, F-symbols, R-symbols, and some other data of the unitary modular tensor category. In this paper, non-Abelian statistics of the Ising anyon is realized using the mixed boundary punctures on the toric code of an Abelian anyon model.

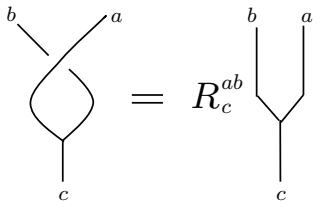


Fig. 1. The braiding operation R_c^{ab}.

Wilczek first discovered the braiding group of a kind of quasiparticle, which gave an additional Aharonov–Bohm phase after the braiding operation.[33,34] These quasiparticles are called Abelian anyons. Immediately after, Kitaev introduced a marvelous exactly solvable model.[1–4] The Kitaev toric code can be viewed as a simplification and generalization of a quantum Z_2 gauge theory. It is a square lattice grid with each edge or vertex hosting a spin-1/2 particle. The grids satisfy periodic boundary conditions forming a torus-like structure. The excitations are Abelian anyons. The vacuum 1, electric charge e, magnetic flux m and fermion $\varepsilon = e \times m$ are four superselection sectors of the Abelian anyons (the case of two mutual antiparticles is ignored here). For Abelian anyons, Chern number $c = 0, 8$ and $c = \pm 4$ are two categories which mod 16. The parameters of the simplest Abelian anyons are those with Chern number $c = 0$, topology spin $\theta = 1$ and Frobenius–Schur indicator $\kappa = 1$. The Abelian anyons are mod 2, and the fusion rules read

$$\begin{aligned} &e \times e = m \times m = \varepsilon \times \varepsilon = 1, \\ &\varepsilon \times e = m, \ \ \varepsilon \times m = e, \ \ e \times m = \varepsilon. \end{aligned} \tag{3}$$

According to the definition of braiding operation (see Fig. 1), the braiding (or exchange) rules of those four superselection sectors are

$$\begin{aligned} &R_{\varepsilon}^{em} = -R_{\varepsilon}^{me} = 1, \\ &R_{e}^{\varepsilon m} = -R_{e}^{m\varepsilon} = 1, \\ &R_{m}^{e\varepsilon} = -R_{m}^{\varepsilon e} = 1, \\ &R_{1}^{ee} = R_{1}^{mm} = -R_{1}^{\varepsilon\varepsilon} = 1. \end{aligned} \tag{4}$$

It is worth noting that the results given by different orders of superscripts on operators are also different. For example, $R_{\varepsilon}^{em} = -R_{\varepsilon}^{me} = 1$. This is not trivial; the representation of another intermediate statistical-Gentile statistics can give a much clearer physical image for the braiding. In the Gentile statistics representation space, R_{ε}^{em} and R_{ε}^{me} are mapped into two mutual conjugate spaces.[35] This kind of anyon is called the Abelian $1/2$-anyons, because the statistical parameter is $1/2$ for winding number 1.

Ising anyons are the simplest non-Abelian anyons. Their Chern number is $c = 1$. Similarly, there are three categories of excitations: the vacuum 1, the Majorana fermion ψ, and the vortex σ. For non-Abelian anyons, the topological spin and the Frobenius–Schur indicators of vortices are divided into 8 pieces $\theta_\sigma = \exp(\mathrm{i}\pi c/8)$ and $\varkappa_\sigma = (-1)^{(c^2-1)/8}$, besides $\theta_1 = 1$, $\theta_\psi = -1$, $\varkappa_1 = \varkappa_\psi = 1$. For Ising anyons, $\theta_\sigma = \exp(\mathrm{i}\pi/8)$ and $\varkappa_\sigma = \varkappa = 1$. The fusion rules of non-Abelian Ising anyons are

$$\psi \times \psi = 1, \quad \psi \times \sigma = \sigma, \quad \sigma \times \sigma = 1 + \psi. \tag{5}$$

And the braiding rules of Ising anyons give

$$\begin{aligned} &R_1^{\psi\psi} = -1, \ \ R_1^{\sigma\sigma} = \varkappa \mathrm{e}^{-\frac{\mathrm{i}\pi c}{8}} = \mathrm{e}^{-\frac{\mathrm{i}\pi}{8}}, \\ &R_\sigma^{\psi\sigma} = R_\sigma^{\sigma\psi} = -\mathrm{i}^c = -\mathrm{i}, \ \ R_\psi^{\sigma\sigma} = \varkappa \mathrm{e}^{\frac{\mathrm{i}3\pi c}{8}} = \mathrm{e}^{\frac{\mathrm{i}3\pi}{8}}. \end{aligned} \tag{6}$$

2.2. Defects on toric code

The toric code can be defined on a lattice with one qubit at each vertex. The Hamiltonian can be expressed as

$$H = -\sum_{v} A_v - \sum_{f} B_f, \tag{7}$$

with stabilizers

$$A_v = \prod_{j\in\partial v} X_j, \quad B_f = \prod_{j\in\partial f} Z_j, \tag{8}$$

where ∂f is the qubits that are connected to the face.[7] The information can be encoded on the toric code by introducing defects on the model surface. Two common kinds of defects are

punctures and twists. Measurements of the stabilizers could disentangle the spin system and create the punctures on the lattice. The logical qubits can be encoded using the parity of the puncture anyons. When Pauli Z stabilizers are measured, electric charge e is excited (the boundary of the puncture is solid). When Pauli X stabilizers are measured, magnetic flux m is excited (the boundary of the puncture is dashed) (see Fig. 2). Twists are extrinsic defects on the toric code. They can be represented by five stabilizer operators $XZYXZ$ which cause a dislocation at the endpoints of the lattice. The anyon braiding around a twist could exchange the type of e and m, while leaving ψ, braiding and fusion rules invariant.[6,7]

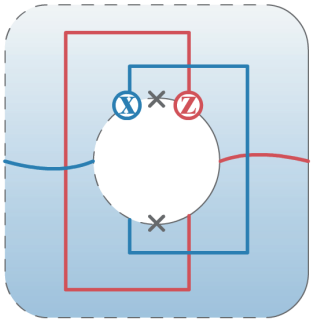


Fig. 2. The mixed boundary punctures model. Z type (red) and X type (blue) strings terminate at solid and dashed boundaries, respectively.[7] Pauli Z and X operators (loops) stabilize this defect. The two horizontal curves represent the stabilizers connecting the boundary and the puncture. The two black crosses at the intersection of the solid boundary and the dashed boundary represent two twists.

In 2022, Benhemou *et al.* designed a new concept of mixed boundary punctures which combined the punctures and twists (Fig. 2).[7] In Fig. 2, half solid and half dashed boundaries are juxtaposed and connected with a pair of twists represented by two crosses. In Ref. [6], Brown had proven the equivalence between the corners of the toric code and twist defects. This mixed boundary corresponds to the measurements of both X and Z stabilizers. The twist applies a Pauli Y operator at each intersection qubit, then the mixed boundary punctures are completed. The strings connecting two mixed boundary punctures indicate that two e or m can be condensed in those two punctures. The string which connects two solid sides represents two e are condensed, while two m correspond to the string connecting two dashed sides (Fig. 3).[7]

2.3. Subspaces of mixed boundary punctures

As Benhemou *et al.* mentioned,[7] the logical qubits are the superposition states in Fig. 3

$$|s_1s_2,\pm\rangle = \frac{|e_1e_2\rangle \pm |m_1m_2\rangle}{\sqrt{2}}. \tag{9}$$

They constructed symmetric states to satisfy the fusion matrix F and braiding evolution matrix B of Ising anyons

$$F = \frac{1}{\sqrt{2}}\begin{pmatrix} 1 & 1 \\ 1 & -1 \end{pmatrix}, \tag{10}$$

$$B = FR^2F^{-1} = \mathrm{e}^{-\mathrm{i}\frac{\pi}{4}}\begin{pmatrix} 0 & 1 \\ 1 & 0 \end{pmatrix}. \tag{11}$$

Actually, we discover that the antisymmetric construction also satisfies the Ising statistics.

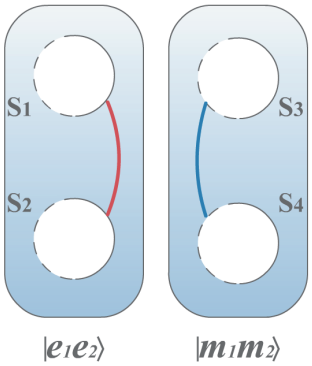


Fig. 3. The states of the mixed boundary punctures. Red string is Z type and blue string is X type. The strings connect the matching boundaries of the puncture pairs. The e and m particles are condensed inside the punctures which means the states of the system are still ground states.

Symmetric subspace In Benhemou's research, they only gave one symmetric construction.[7] The basic units of the Ising statistics on the toric code are the joint states of two symmetric states $|(s_1s_2,+)(s_1s_2,+)\rangle$ or $|(s_1s_2,-)(s_1s_2,-)\rangle$. They proved that this symmetric construction satisfied the fusion matrix F and braiding evolution matrix B of Ising anyons. In Fig. 4, braiding s_1 around s_3 brings different results. When s_1 and s_3 condense the same kind of quasiparticles, braiding creates the same operator loops enclosing the punctures to the strings. For example, in Figs. 4(a) and 4(b), s_1 and s_3 are both $e(m)$ particles, and the strings are $Z(X)$-type stabilizers. Braiding s_1 around s_3 gives both s_1 and s_3 a $Z(X)$ loop crossing the $Z(X)$ string. When s_1 and s_3 condense different kinds of quasiparticles, braiding creates different operator loops enclosing the punctures to the strings. For instance, in Figs. 4(c) and 4(d), s_1 and s_3 are $e(m)$ and $m(e)$,respectively, and the strings are $Z(X)$-type and $X(Z)$-type stabilizers. Braiding s_1 around s_3 gives s_1 and s_3 $X(Z)$ and $Z(X)$ loops crossing the $Z(X)$ and $X(Z)$ strings.

The Pauli X operation corresponds to two braiding operations B^2. The Pauli X operation can be realized by

(i) As described in Benhemou *et al.*, braiding puncture s_1 around s_3 once.

(ii) If the particle types in s_1 and s_2 are the same as those in s_3 and s_4, the result corresponds to Figs. 4(a) and 4(b).

(iii) If the particle types in s_1 and s_2 differ from those in s_3 and s_4, the result corresponds to Figs. 4(c) and 4(d), which implies the introduction of a minus sign.

The realization of the Pauli Z operation is

(i) Creating a pair of ψ in s_1 and s_2 (exchange e_1e_2 and m_1m_2).

(ii) Or another method is creating a pair of ψ in s_3 and s_4 (exchange e_3e_4 and m_3m_4) (Fig. 5(a)).[7]

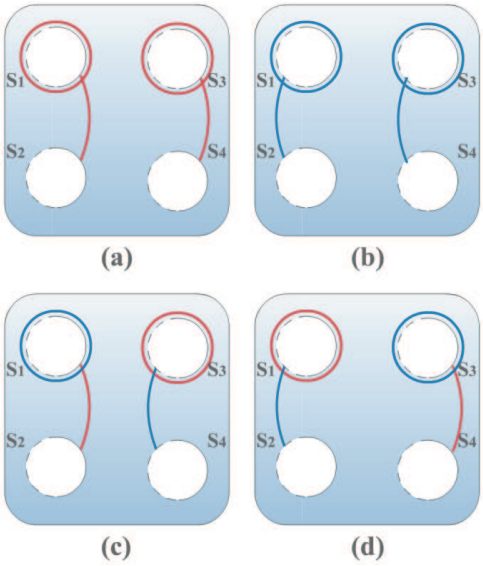


Fig. 4. The basic units of the Ising statistics on toric code. Braiding s_1 around s_3 brings different results. Panels (a) and (b) are trivial, loops and strings are the same type. In panels (c) and (d), loops and strings are different types, which give minus signs.

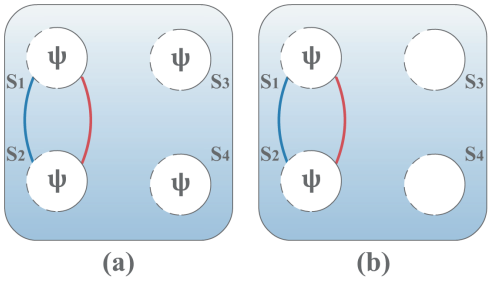


Fig. 5. The realization of Pauli Z operation. Panels (a) is the Pauli Z in the symmetric subspace, while panel (b) is the Pauli Z in the antisymmetric subspace.

Antisymmetric subspace In this part, we discuss the antisymmetric construction of the mixed boundary punctures on the toric code. We prove that this mixed boundary punctures model also satisfies the Ising statistics in the antisymmetric subspace $\{|(s_1s_2,+)(s_3s_4,-)\rangle, |(s_1s_2,-)(s_3s_4,+)\rangle\}$. As mentioned earlier, we need at least four mixed boundary punctures to show the Ising statistics. In the antisymmetric subspace, the basic vectors are

$$\begin{aligned}&|(s_1s_2,+)(s_3s_4,-)\rangle \equiv |+-\rangle\\ =&\frac{1}{2}(|e_1e_2e_3e_4\rangle - |e_1e_2m_3m_4\rangle\\ &+|m_1m_2e_3e_4\rangle - |m_1m_2m_3m_4\rangle), \qquad (12)\\ &|(s_1s_2,-)(s_3s_4,+)\rangle \equiv |-+\rangle\\ =&\frac{1}{2}(|e_1e_2e_3e_4\rangle + |e_1e_2m_3m_4\rangle\\ &-|m_1m_2e_3e_4\rangle - |m_1m_2m_3m_4\rangle). \qquad (13)\end{aligned}$$

It can be easily proved that the action of the fusion matrix is

$$F|+-\rangle = \frac{1}{\sqrt{2}}(|e_1e_2e_3e_4\rangle - |m_1m_2m_3m_4\rangle) = |1_{13}1_{24}\rangle, \qquad (14)$$

$$F|-+\rangle = \frac{1}{\sqrt{2}}(-|e_1e_2m_3m_4\rangle + |m_1m_2e_3e_4\rangle) = |\psi_{13}\psi_{24}\rangle, \qquad (15)$$

where we define the vacuum and the Majorana fermion states

$$\begin{aligned}|1_{13}1_{24}\rangle &= \frac{1}{\sqrt{2}}(|e_1e_2e_3e_4\rangle - |m_1m_2m_3m_4\rangle),\\ |\psi_{13}\psi_{24}\rangle &= \frac{1}{\sqrt{2}}(-|e_1e_2m_3m_4\rangle + |m_1m_2e_3e_4\rangle), \qquad (16)\end{aligned}$$

so the basic vectors

$$\begin{aligned}|+-\rangle &= \frac{1}{\sqrt{2}}(|1_{13}1_{24}\rangle + |\psi_{13}\psi_{24}\rangle),\\ |-+\rangle &= \frac{1}{\sqrt{2}}(|1_{13}1_{24}\rangle - |\psi_{13}\psi_{24}\rangle). \qquad (17)\end{aligned}$$

When the braiding operation acts on those two states, we have

$$B_{13}^2|+-\rangle = |-+\rangle, \quad B_{13}^2|-+\rangle = |+-\rangle, \qquad (18)$$

where B_{13}^2 means braiding particle 1 around particle 3, and it is a Pauli X operation obviously. But the Pauli Z operation is different from the symmetric case. In the antisymmetric subspace, the Pauli Z operation is the process of creating a pair of ψ in s_1 and s_2 (Fig. 5(b)). After that, the states are

$$Z|+-\rangle = |+-\rangle, Z|-+\rangle = -|-+\rangle. \qquad (19)$$

What calls for special attention is that ψ is the fermion ε in the toric code; their single particle fusion and braiding rule follow Eq. (3), but the total effect of the states $\{|+-\rangle, |-+\rangle\}$ satisfies the Ising statistics Eqs. (10) and (11).

Ising anyons do not inherently support a T gate ($\pi/8$ gate), which limits their braiding operations to the Clifford group and renders them non-universal for quantum computation. This limitation can be addressed through the introduction of magic state distillation — a fault-tolerant protocol that prepares high-fidelity magic states using Clifford operations, which can then be combined with braiding to implement T gates. However, this approach incurs substantial resource overhead due to the need for distillation factories and multiple distillation rounds.[31]

A more elegant solution has recently emerged from research led by the University of Southern California. Within the framework of non-semisimple topological quantum field theory, the team discovered a new anyon type — termed the "neglecton" — which was previously discarded in conventional semisimple models due to its zero quantum trace. Remarkably, by introducing just a single stationary neglecton, Ising anyons can achieve universal quantum computation through braiding alone. The neglecton serves as a fixed point around which Ising anyons are braided, enabling a complete set of quantum gates. While the non-semisimple framework initially raised concerns about unitarity violations, the researchers developed

a "local isolation" strategy that confines quantum information to structurally sound regions of the theory, effectively quarantining the problematic mathematical aspects. This breakthrough transforms previously "neglected" mathematical components into a powerful resource for universal topological quantum computing, though experimental realization remains an open challenge.[36]

3. Fault-tolerant properties

The mixed boundary punctures model is a simulation of Ising anyon statistical properties, not real Ising anyons. Non-Abelian anyons are intrinsically fault-tolerant, because the Hilbert space of non-Abelian anyons is composed of the local subspace and the logical subspace. Errors only exist in the local subspace, which is isolated from the logical subspace. The logical subspace is determined by the conjugacy class of a finite group and the irreducible representation of its centralizer. Local operations cannot access the logical subspace, so quantum information is protected from local errors. Is this simulation immune to noise? We consider two typical noises: the collective dephasing noise and the collective rotation noise. We confirm to the extent that the symmetric subspace $\{|{+}{+}\rangle, |{-}{-}\rangle\}$ and the antisymmetric subspace $\{|{+}{-}\rangle, |{-}{+}\rangle\}$ of the mixed boundary punctures model can be regarded as two logical subspaces of Ising anyons.

Collective dephasing noise and collective rotation noise are of fundamental importance in quantum information science because they represent the most physically relevant and challenging types of correlated errors in practical quantum systems. These noise models directly capture realistic decoherence mechanisms: collective dephasing arises from global field fluctuations that randomly rotate qubit phases, while collective rotation models uniform control errors that simultaneously rotate all qubits.[37] Their significance stems from the fact that they violate the core assumption of standard quantum error correction codes — namely, that errors are independent and stochastic. Correlated noise can cause logical errors to accumulate in ways that are not captured by conventional threshold analyses, making systems that are immune to such noise particularly valuable.[38] Furthermore, in quantum communication protocols, these two noise types serve as the standard benchmarks for evaluating practical applicability, as they dominate decoherence in fiber-based and solid-state implementations. Demonstrating fault-tolerance against these specific noise models therefore provides strong evidence that a quantum information scheme possesses genuine physical robustness beyond what is guaranteed by standard error correction alone.

3.1. Dephasing noise

We assume $|0\rangle = |e\rangle$ and $|1\rangle = |m\rangle$ on the toric code. The collective dephasing noise gives

$$U_{\rm d}|e\rangle = |e\rangle, \quad U_{\rm d}|m\rangle = {\rm e}^{{\rm i}\phi(t)}|m\rangle, \tag{20}$$

where $\phi(t)$ is a random phase that varies over time.

(i) The symmetric subspace $\{|{+}{+}\rangle, |{-}{-}\rangle\}$.

According to Eqs. (9) and (20), in the two-qubit case, we have

$$\underset{2}{\otimes} U_{\rm d}|\pm\rangle = \frac{1}{\sqrt{2}}(|e_1e_2\rangle \pm {\rm e}^{{\rm i}2\phi}|m_1m_2\rangle) \equiv |\mp\rangle. \tag{21}$$

In the symmetric subspace, when the collective dephasing noise operator acts on the basic unit of the Ising anyons (4 mixed boundary punctures), the states become

$$\begin{aligned}\underset{4}{\otimes} U_{\rm d}|\pm\pm\rangle \;=\; & \frac{1}{2}(|e_1e_2e_3e_4\rangle \pm {\rm e}^{{\rm i}2\phi}|e_1e_2m_3m_4\rangle \\ & \pm {\rm e}^{{\rm i}2\phi}|m_1m_2e_3e_4\rangle \\ & + {\rm e}^{{\rm i}4\phi}|m_1m_2m_3m_4\rangle) \equiv |\mp\mp\rangle. \end{aligned}\tag{22}$$

By calculation, it can be proven that $\langle\tilde{\mp}\tilde{\mp}|\tilde{-}\tilde{-}\rangle = 0$ and $\langle\mp\mp|\mp\mp\rangle = 1$. The system in the symmetric subspace is immune to the collective dephasing noise.

(ii) The antisymmetric subspace $\{|{+}{-}\rangle, |{-}{+}\rangle\}$.

Similar to the symmetric subspace, under the effect of the collective dephasing noise, the four qubit states become

$$\begin{aligned}&\underset{4}{\otimes} U_{\rm d}|\pm\mp\rangle = \frac{1}{2}(|e_1e_2e_3e_4\rangle \mp {\rm e}^{{\rm i}2\phi}|e_1e_2m_3m_4\rangle \\ &\pm {\rm e}^{{\rm i}2\phi}|m_1m_2e_3e_4\rangle - {\rm e}^{{\rm i}4\phi}|m_1m_2m_3m_4\rangle) \equiv |\mp\tilde{\mp}\rangle. \end{aligned}\tag{23}$$

It is easy to verify that $\langle\tilde{\mp}\tilde{-}|\tilde{-}\tilde{\mp}\rangle = 0$ and $\langle\mp\tilde{\mp}|\mp\tilde{\mp}\rangle = 1$. The system in the antisymmetric subspace is immune to the collective dephasing noise.

3.2. Rotation noise

The collective rotation noise affects the states as

$$\begin{aligned}U_{\rm r}|e\rangle &= \cos\theta|e\rangle + \sin\theta|m\rangle, \\ U_{\rm r}|m\rangle &= -\sin\theta|e\rangle + \cos\theta|m\rangle, \end{aligned}\tag{24}$$

where $\theta(t)$ is also a random phase that varies over time.

(i) The symmetric subspace $\{|{+}{+}\rangle, |{-}{-}\rangle\}$.

In the symmetric subspace, according to Eq. (24), it is not difficult to draw the conclusion that $|{+}{+}\rangle$ is invariant under the collective rotation noise

$$\begin{aligned}\underset{4}{\otimes} U_{\rm r}|{+}{+}\rangle \;=\; & \frac{1}{2}(|e_1e_2e_3e_4\rangle + |e_1e_2m_3m_4\rangle + |m_1m_2e_3e_4\rangle \\ & + |m_1m_2m_3m_4\rangle) \equiv |\tilde{+}\tilde{+}\rangle. \end{aligned}\tag{25}$$

Another state is slightly more complex than

$$\begin{aligned}&\underset{4}{\otimes} U_{\rm r}|{-}{-}\rangle = \frac{1}{2}[\prod_{p=1}^{4}(\cos\theta|e_p\rangle + \sin\theta|m_p\rangle) \\ &- \prod_{p=1}^{2}\prod_{q=3}^{4}(\cos\theta|e_p\rangle + \sin\theta|m_p\rangle)(-\sin\theta|e_q\rangle + \cos\theta|m_q\rangle)\end{aligned}$$

$$-\prod_{p=1}^{2}\prod_{q=3}^{4}(-\sin\theta\,|e_p\rangle+\cos\theta\,|m_p\rangle)(\cos\theta\,|e_q\rangle+\sin\theta\,|m_q\rangle)$$

$$+\prod_{p=1}^{4}(-\sin\theta\,|e_p\rangle+\cos\theta\,|m_p\rangle)]\equiv|\tilde{-}\tilde{-}\rangle\,. \tag{26}$$

After a series of derivations, we have proved that $\langle\tilde{\mp}\tilde{\mp}\,|\tilde{-}\tilde{-}\rangle=0$ and $\langle\tilde{\pm}\tilde{\pm}\,|\tilde{\pm}\tilde{\pm}\rangle=1$ under the collective rotation noise. Therefore, symmetric subspaces can resist the collective rotation noise.

(ii) The antisymmetric subspace $\{|+-\rangle,|-+\rangle\}$.

In the case of the antisymmetric subspace, under the actions of the collective rotation noise, the basic vectors become

$$\begin{aligned}\underset{4}{\otimes}U_{\rm r}\,|+-\rangle=\frac{1}{2}\Bigg[&\prod_{p=1}^{4}(\cos\theta\,|e_p\rangle+\sin\theta\,|m_p\rangle)\\&-\prod_{p=1}^{2}\prod_{q=3}^{4}(\cos\theta\,|e_p\rangle+\sin\theta\,|m_p\rangle)(-\sin\theta\,|e_q\rangle+\cos\theta\,|m_q\rangle)\\&+\prod_{p=1}^{2}\prod_{q=3}^{4}(-\sin\theta\,|e_p\rangle+\cos\theta\,|m_p\rangle)(\cos\theta\,|e_q\rangle+\sin\theta\,|m_q\rangle)\\&-\prod_{p=1}^{4}(-\sin\theta\,|e_p\rangle+\cos\theta\,|m_p\rangle)\Bigg]\equiv|\tilde{\mp}\tilde{-}\rangle\,,\end{aligned} \tag{27}$$

$$\begin{aligned}\underset{4}{\otimes}U_{\rm r}\,|-+\rangle=\frac{1}{2}\Bigg[&\prod_{p=1}^{4}(\cos\theta\,|e_p\rangle+\sin\theta\,|m_p\rangle)\\&+\prod_{p=1}^{2}\prod_{q=3}^{4}(\cos\theta\,|e_p\rangle+\sin\theta\,|m_p\rangle)(-\sin\theta\,|e_q\rangle+\cos\theta\,|m_q\rangle)\\&-\prod_{p=1}^{2}\prod_{q=3}^{4}(-\sin\theta\,|e_p\rangle+\cos\theta\,|m_p\rangle)(\cos\theta\,|e_q\rangle+\sin\theta\,|m_q\rangle)\\&-\prod_{p=1}^{4}(-\sin\theta\,|e_p\rangle+\cos\theta\,|m_p\rangle)\Bigg]\equiv|\tilde{-}\tilde{\mp}\rangle\,.\end{aligned} \tag{28}$$

We can still prove that the inner product remains invariant under the collective rotation noise. We have $\langle\tilde{\mp}\tilde{-}\,|\tilde{-}\tilde{\mp}\rangle=0$ and $\langle\tilde{\pm}\tilde{\mp}\,|\tilde{\pm}\tilde{\mp}\rangle=1$. The antisymmetric subspace is an invariant subspace under the collective rotation noise.

4. Information masking

Quantum information masking is a unique property of multi-body systems in which quantum information is stored in the correlations between subsystems rather than within them. It arises from the quantum entanglement among these subsystems. The no-masking theorem proposed by Modi *et al.* is one of the family of no-go theorems.[39] Li *et al.* proposed an interesting three-body information masking scheme that utilizes the properties of Latin squares in mathematics.[40] Then we simulated the quantum information masking process in Abelian anyon system and Ising anyon system according to Li *et al.*'s Latin squares scheme.[41] Here, using the mixed boundary punctures model, Ising anyon statistics are simulated on toric code. We discuss the Latin squares scheme of quantum information masking process under this model.

In this case, we need three pairs of mixed boundary punctures (six holes, Fig. 6), which corresponds to three Ising anyons. In our previous work, we proved that the three-partite quantum information masking scheme maps the arbitrary state $\alpha\,|1\rangle+\beta\,|\psi\rangle+\gamma|\sigma\rangle$ as

$$\begin{aligned}|\Psi\rangle\;=\;&\frac{1}{\sqrt{3}}[\alpha\,|111\rangle+\alpha\,|\psi\psi\psi\rangle+\alpha\,|\sigma\sigma\sigma\rangle\\&+\beta\,|1\sigma\psi\rangle+\beta\,|\psi1\sigma\rangle+\beta\,|\sigma\psi1\rangle\\&+\gamma|1\psi\sigma\rangle+\gamma|\psi\sigma1\rangle+\gamma|\sigma1\psi\rangle].\end{aligned} \tag{29}$$

In this case, we can get $\mathrm{Tr}_{AB}(|\Psi\rangle\langle\Psi|)=\mathrm{Tr}_{AC}(|\Psi\rangle\langle\Psi|)=\mathrm{Tr}_{BC}(|\Psi\rangle\langle\Psi|)=I/3$; the masking process is accomplished, and the information is stored in the quantum correlation rather than the subsystems. Please refer to our work for the specific proof process. All terms in the braiding operation satisfy the masking requirement obviously except for the three Ising anyons term $|\sigma\sigma\sigma\rangle$. The braiding operation gives each term an additional phase which can cancel each other in the calculation of $|\Psi\rangle\langle\Psi|$. According to the special statistical properties Eqs. (5) and (6), the case of term $|\sigma\sigma\sigma\rangle$ is a little complicated. In the mixed boundary punctures model, we assume three pairs of mixed boundary punctures to realize the three Ising anyon state $|\sigma\sigma\sigma\rangle$.

We give an example of the state $|\pm\pm\pm\rangle$, other cases $|\pm\mp\pm\rangle$ and $|\pm\pm\mp\rangle$ are the same,

$$\begin{aligned}|\pm\pm\pm\rangle\;=\;&+|e_1e_2e_3e_4e_5e_6\rangle\pm|e_1e_2e_3e_4m_5m_6\rangle\\&\pm|e_1e_2m_3m_4e_5e_6\rangle+|e_1e_2m_3m_4m_5m_6\rangle\\&\pm|m_1m_2e_3e_4e_5e_6\rangle+|m_1m_2e_3e_4m_5m_6\rangle\\&+|m_1m_2m_3m_4e_5e_6\rangle\pm|m_1m_2m_3m_4m_5m_6\rangle\,.\end{aligned} \tag{30}$$

We assume $M_1=|e_1e_2e_3e_4e_5e_6\rangle\pm|m_1m_2m_3m_4m_5m_6\rangle$, $M_2=\pm|e_1e_2e_3e_4m_5m_6\rangle+|m_1m_2m_3m_4e_5e_6\rangle$, $M_3=+|e_1e_2m_3m_4m_5m_6\rangle\pm|m_1m_2e_3e_4e_5e_6\rangle$ and $M_4=\pm|e_1e_2m_3m_4e_5e_6\rangle+|m_1m_2e_3e_4m_5m_6\rangle$. The braiding operation between Ising anyons 1 and 3 named B_{13} gives M_3 and M_4 a minus sign and keeps M_1 and M_2 invariant. Similarly, the braiding operation between Ising anyons 3 and 5 named B_{35} gives M_2 and M_4 a minus sign and keeps M_1 and M_3 invariant. B_{13} and B_{35} are both adjacent braidings of Ising anyons. It is not difficult to prove that, in the adjacent braiding case, the minus signs can offset each other. There is another more complicated braiding type, three-partite braiding. For instance, braiding σ_1 around σ_2 and σ_3 corresponds to braiding s_1 around s_3 and s_5. Three-partite braiding which has the same beginning and end particle positions has two styles (Fig. 7). In Fig. 7(a), particle 2 and 3 do not braid, $B=B_{13}B_{15}B_{51}B_{31}$ is composed of four adjacent braidings. In Fig. 7(b), particles 2 and 3 also braid, the diagram has two links. If we define the

braiding B' as a cyclic permutation, then B'^3 gives the same extreme points of the strands. These two braiding styles are quite different obviously, which makes the problem more difficult. Fortunately, the three-partite system is an Ising anyon system. In Yu's research,[42] it has been proven that the braiding of Ising anyons is only related to the endpoints of strands, since the braiding group is a subgroup of the Clifford group, which is a finite group. It is noteworthy that this conclusion applies only to Ising anyons. The braiding groups of other anyons are infinite groups and heavily depend on the manner of braiding. Thus the two diagrams in Fig. 7 are the same $B = B'$ here, we can conclude them as Fig. 8 in which the braiding process is a black box. Therefore, the braiding of three-partite is equivalent to the successive action of adjacent braiding which can realize the quantum information masking as mentioned above.

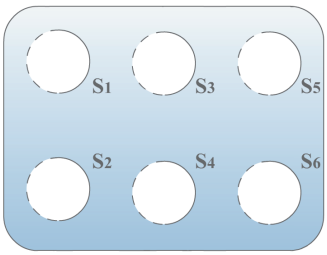


Fig. 6. Six mixed boundary punctures model simulates three-Ising-anyon state.

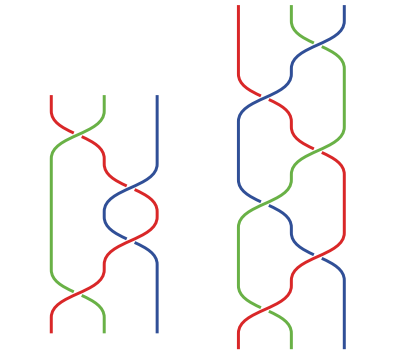


Fig. 7. Two different braiding styles give the same extreme points of the strands. These two distinct braiding styles lead to two fundamentally different definitions of identity.

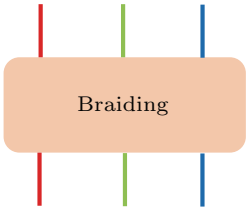


Fig. 8. The simplified model of braiding in Ising anyon system. The braiding of Ising anyons is only related to the endpoints of strands, since the braiding group is a subgroup of the Clifford group.[42]

5. Feasibility analysis

To evaluate the practical feasibility of our proposed scheme, we provide a brief analysis of its resource overhead. In surface-code-based architectures, the number of physical qubits required to implement a fault-tolerant logical qubit is strongly dependent on the specific hardware platform and error-correction protocol. Theoretically, a logical qubit with code distance d requires at least $2d^2$ physical qubits in the ideal case.[3] However, when practical considerations such as dual-rail encoding, magic state distillation factories, and qubit routing are taken into account, the typical resource requirement increases to approximately $20d^2$ physical qubits per logical qubit. In our model, each logical qubit is encoded using a pair of mixed-boundary punctures, leading to an estimated physical overhead of about $40d^2$ physical qubits per logical qubit. For a quantum register consisting of n logical qubits, the total number of physical qubits therefore scales as $O(nd^2)$. Regarding temporal overhead, logical gate operations in our scheme are implemented via braiding sequences of Ising anyons. All Clifford gates can be realized with a constant number of braiding operations, consistent with the theoretical predictions for topological quantum computation. A key advantage of our approach over non-topological schemes lies in its inherent robustness: the fidelity of logical gates is determined by the topological properties of the system and the code distance d, rather than by the precision of external control pulses. It is worth noting, however, that the implementation of non-Clifford gates (e.g., the T gate), which are essential for achieving universal quantum computation, necessitates the use of magic state distillation. This requirement introduces substantial additional spatial and temporal overhead — a challenge common to all Ising-anyon-based quantum computing platforms.[38]

6. Summary

The toric code, also known as the surface code, is a renowned topological anyon model proposed by Kitaev. Defects within the toric code can exhibit non-Abelian statistical properties, enabling the potential for topological quantum computation. The defects can be classified into punctures and twists. Benhemou *et al.* hybridized these two types of defects into the mixed boundary punctures model, combining their advantages. This mixed boundary punctures model demonstrates the non-Abelian statistics of Ising anyons. They proposed that non-Abelian statistical properties could be realized within the symmetric subspace, but we have demonstrated that the antisymmetric subspace can also exhibit these properties.

Given that this mixed boundary punctures model can simulate the statistical properties of Ising anyons on the toric code, we investigate whether it also possesses fault tolerance similar to that of non-Abelian anyons. We delve into two typical types of noise and find that the mixed boundary punctures model is immune to these disturbances. Furthermore, we demonstrate that this system can achieve quantum information masking

by storing information in the correlations between subsystems rather than within the subsystems themselves.

Acknowledgments

Project supported by the Fundamental Research Funds for the Central Universities, China (Grant No. 2022JKF02024) and the National Natural Science Foundation of China (Grant No. 11675119).

References

[1] Kitaev A Y 1997 *Russ. Math. Surv.* **52** 1191
[2] Kitaev A Y 2001 *Phys. Usp.* **44** 131
[3] Kitaev A Y 2003 *Ann. Phys.* **303** 2
[4] Kitaev A Y 2006 *Ann. Phys.* **321** 2
[5] Kells G, Slingerland J K and Vala J 2009 *Phys. Rev. B* **80** 125415
[6] Brown B J, Laubscher K, Kesselring M S and Wootton J R 2017 *Phys. Rev. X* **7** 021029
[7] Benhemou A, Pachos J K and Browne D E 2022 *Phys. Rev. A* **105** 042417
[8] Pachos J K 2012 *Introduction to Topological Quantum Computation* (Cambridge: Cambridge University Press)
[9] Ogburn R W and Preskill J 1999 *Quantum Computing and Quantum Communications* (Berlin: Springer) pp. 341–356
[10] Fu L and Kane C L 2008 *Phys. Rev. Lett.* **100** 096407
[11] Rajpoot G, Kumari K and Jain S R‘ 2024 *Eur. Phys. J. Spec. Top.* **233** 1341
[12] Xu S B, Sun Z Z, Wang K et al. 2023 *Chin. Phys. Lett.* **40** 060301
[13] Trinca C C, Interlando J C, Palazzo R Jr, de Andrade A A and Watanabe R A 2023 *Quantum Inf. Process.* **22** 213
[14] Manoj N and Shenoy V B 2023 *Phys. Rev. B* **107** 165136
[15] Li A Q, Tian C W, Xu X X, Ma H Y and Liang J Q 2025 *Chin. Phys. B* **34** 030306
[16] Li F, Li A Q, Gan Q D and Ma H Y 2024 *Chin. Phys. B* **33** 040307
[17] Ji N H, Sun H Q, Xiao B, Song P L and Ma H Y 2025 *Chin. Phys. B* **34** 020309
[18] Raussendorf R, Harrington J and Goyal K 2006 *Ann. Phys.* **321** 2242
[19] Raussendorf R and Harrington J 2007 *Phys. Rev. Lett.* **98** 190504
[20] Bombin H and Martin-Delgado M A 2008 *Phys. Rev. B* **78** 165128
[21] Fowler A G, Stephens A M and Groszkowski P 2009 *Phys. Rev. A* **80** 052312
[22] Brell C G 2015 *New J. Phys.* **17** 023029
[23] Bombin H 2010 *Phys. Rev. Lett.* **105** 030403
[24] Barkeshli M, Jian C M and Qi X L 2013 *Phys. Rev. B* **87** 045130
[25] Hastings M B and Geller A 2015 *Quantum Inf. Comput.* **15** 0962
[26] Wootton J R 2015 *J. Phys. A* **48** 215302
[27] Teo J C Y 2016 *J. Phys.: Condens. Matter* **28** 143001
[28] Zheng H, Dua A and Jiang L 2015 *Phys. Rev. B* **92** 245139
[29] Krishna A and Poulin D 2020 *Phys. Rev. Research* **2** 023116
[30] Kitaev A Y 1997 *Proc. Third Int. Conf. Quantum Communication, Computing and Measurement* (New York: Plenum Press)
[31] Freedman M H, Larsen M and Wang Z 2002 *Commun. Math. Phys.* **227** 605
[32] Dai H N, Yang B, Reingruber A, Sun H, Xu X F, Chen Y A, Yuan Z S and Pan J W 2017 *Nat. Phys.* **13** 1195
[33] Wilczek F 1982 *Phys. Rev. Lett.* **48** 1144
[34] Wilczek F 1982 *Phys. Rev. Lett.* **49** 957
[35] Shen Y, Zhang F L, Chen Y Z and Zhou C C 2023 *Physica A* **612** 128495
[36] Iulianelli F, Kim S, Sussan J and Lauda A D 2025 *Nat. Commun.* **16** 6408
[37] Wang X B 2009 *Opt. Commun.* **282** 4171
[38] Zhao Y and Liu D E 2025 *PNAS Nexus* **4** pgaf063
[39] Modi K, Pati A K, Sen A and Sen U 2018 *Phys. Rev. Lett.* **120** 230501
[40] Li M S and Wang Y L 2018 *Phys. Rev. A* **98** 062306
[41] Shen Y, Shang W M, Zhou C C and Zhang F L 2024 *Phys. Rev. A* **109** 032421
[42] Yu L W 2018 *Quantum Inf. Process.* **17** 44